Resolving multiple rescatterings in high-order-harmonic generation

Carlos Hernández-García and Luis Plaja

Resolving multiple rescatterings in high-order harmonic generation

Carlos Hernández-García[1,2,*] and Luis Plaja[1]

[1]*Grupo de Investigación en Aplicaciones del Láser y Fotónica,*
Universidad de Salamanca, E-37008, Salamanca, Spain
[2]*JILA, University of Colorado at Boulder, Boulder, Colorado 80309-0440, USA*

We explore the conditions for resolving high-order electronic recollisions in high-order harmonic spectroscopy. We identify intrinsic phase mismatch and time-frequency uncertainty as the two fundamental limitations against the spectral distinguishability of these multiple rescatterings. Our numerical computations show that flat top mid-infrared driving fields are the optimal candidates for the study of multiple recollision phenomena.

I. INTRODUCTION

High-order harmonic generation (HHG) [1, 2] is considered one of the most suitable methods to generate coherent light from the extreme-ultraviolet (XUV) to the x-ray regime [3]. It is a highly nonlinear process that can be nicely explained in semiclassical terms, with the so-called three-step model [4, 5]. In the first step, the atomic electron is tunnel-ionized through the Coulomb potential barrier, deformed by the intense laser field. After the release, the electronic wave packet is accelerated by the laser field and driven back towards the parent ion. In a final step, upon rescattering with the parent ion, the kinetic energy acquired by the electron during its excursion is released in the form of harmonics. Interestingly, this coherent high-frequency radiation is known to be emitted in the form of ultrashort pulses of attosecond duration [6–8].

The emission of radiation at a given harmonic order is built from the coherent addition of a set of rescattering events of the same energy [9, 10]. From these, the most efficient are those corresponding to first-time recollisions, as the electron excursion times are shorter and, therefore, the electronic wavepacket is less spread. Every half cycle of the driving laser pulse, two paths lead to first-time recollisions of the same energy, named according to their particular excursion time as *short* and *long*. High-order recollisions (HOR) take place after excursion times longer than the laser period and, hence, they have a secondary weight in the overall harmonic spectrum. Figure 1a shows the rescattering trajectories corresponding to electrons ionized during half cycle of the laser field. The trajectory highlighted in blue leads to the most energetic recollision, and it is responsible for the emission of the highest frequency harmonics. Note that trajectories involving multiple rescatterings correspond to electronic wave packets ionized before those leading to the most energetic path.

There are different reasons why HOR are potentially interesting. It has been demonstrated recently that multiple path interference introduces an ultrafast modulation in the attosecond pulses, that can reach the zeptosecond time scale when using mid-infrared (mid-IR) driving fields [11]. For instance, there is a great interest in the development of ultrafast mid-IR sources [12–14], which allow to extend HHG radiation into the x-ray regime [3, 15–18]. On the other hand, longer excursion times make these trajectories more sensitive to the details of the Coulomb potential, through the accumulated phase, extending the time interval for sampling, and thus allowing to capture multi-femtosecond dynamics through high-order harmonic spectroscopy [19]. HOR are also known to contribute to the structure of the low energy part of the non-angle resolved photoelectron spectra induced by mid-IR fields [20–23], and recent experiments reported their signature in the photoelectron angular distributions [24]. Although the influence of HOR in the HHG process has been long discussed [25–27], there is still no experimental evidence of them. A recent study points out that HOR are particularly sensitive to phase matching during harmonic propagation in macroscopic targets and that, when using Gaussian driving beams, their contribution is suppressed [28]. On the other hand, it has been pointed out that HOR will have an increasingly distinct role in the high-order harmonic spectrum as the driving wavelength is shifted to the mid-IR [11, 29, 30].

The aim of this paper is to identify the conditions under which HOR can be resolved in a HHG experiment. To this end, we present in section II the signatures of HOR in HHG, and perform macroscopic HHG simulations using Gaussian, Bessel and flat-top driving beams. Our results indicate that flat-top beams are optimal for resolving HOR. Afterwards in section III we analyze the effect of different driving wavelengths, and perform a quantitative analysis to show that long wavelength driving lasers are required to identify HOR in HHG. Finally, we show that HOR imprint a clear signature in the HHG spectrum of isolated attosecond pulses.
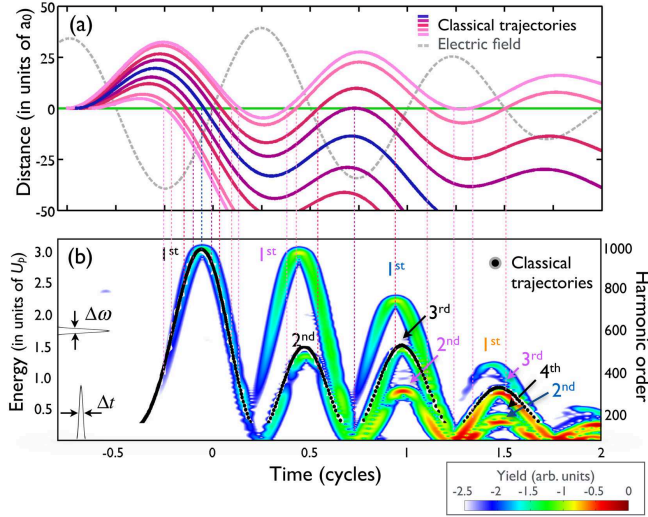
* carloshergar@usal.es

FIG. 1. (Color online) (a) Sample of electronic trajectories in a 6-cycle (full width) laser field with a $\cos^2$-envelope. The grey-dashed line represents the electric field in arbitrary units and the green line indicates the core position. Four pairs of trajectories are represented for energies at first-order recollision of $2.9U_p$ (purple), $2.5U_p$ (dark pink), $1.5U_p$ (pink), and U_p (light pink), whereas the most energetic trajectory, raising $3.17U_p$ at the first recollision, is represented in blue. The vertical axis represents the distance from the core in atomic units (a_0). (b) Time-frequency analysis for the HHG spectrum obtained solving TDSE in helium (color background). The laser pulse is modeled as in panel (a) with a wavelength of $2~\mu m$ and peak intensity of $5 \times 10^{14}~W/cm^2$. We use a Gaussian window with spectral FWHM of $\Delta\omega = 10\omega_0$, (where ω_0 is the fundamental frequency), which corresponds to a temporal FWHM of $\Delta t = T/11.4$, where T is the laser period. The photon energy of the harmonics is given in terms of the rescattering energy (in units of U_p, left vertical axis), and in terms of the harmonic order (right vertical axis). The classical returning kinetic energies at the instant of recollision are shown in black dots for the electrons ionized in the temporal interval between -0.75T and -0.5T. The labels in different colors represent the families of rescattering events that correspond to the wave-packet that was ionized during the same half-cycle.

II. OPTIMIZED PHASE MATCHING OF HIGH-ORDER RESCATTERINGS.

A. Contribution of HOR to the high-order harmonic spectrum.

Figure 1b presents the results of a single-atom HHG calculation, using a time-frequency description of the harmonic emission [31]. The data shown correspond to the numerical integration of the 3D time-dependent Schrödinger equation (TDSE) in helium for a 6 cycles (full-width) $\cos^2$ envelope of a sin carrier wave of $2~\mu m$ wavelength and peak intensity of 5×10^{14} W/cm^2. The calculations consider a single-active electron interacting

with an effective potential obtained from density functional computations [32, 33].

The time-frequency analysis shows the instants when a particular region of the spectrum has been emitted. The FWHM widths of the spectral and temporal amplitude windows, $\Delta\omega$ and Δt, which determine the resolution in frequency and time respectively, are related by $\Delta t = 5.55/\Delta\omega$. As it is usually observed in HHG calculations, the time evolution of the harmonic emission follows faithfully the distribution of rescattering energies of classical trajectories (black dots in Fig. 1b), allowing to identify the different contributions to the harmonic emission of classical paths in Fig. 1a. The contribution of rescatterings of increasing order appears in a time-ordered sequence, as the excursion time associated to each order increases monotonically. After a few cycles, the harmonic radiation contains the contribution of rescatterings of different orders, at different energies. Note that the classical rescattering energies are scale invariant in ponderomotive energy units (in atomic units, $U_P = Ic^2\lambda^2/16\pi^2$, I being the laser intensity, c the velocity of light and λ the laser wavelength).

B. Spatial beam profiles for optimized HOR phase-matching: Bessel and flat-top beams.

HHG from macroscopic targets can be intricate, as it depends not only on the single-atom response, but also on how the harmonics from the elementary radiators interfere [34, 35]. Phase matching plays an essential role, limiting the volume at the target in which the harmonics are generated efficiently. The phase of the high-order harmonics is known to depend on the details of the electron paths. In particular, the sensitivity of the phase to changes in the driving field increases for longer excursion times. Therefore HOR contributions to HHG can be easily phase mismatched, and their contribution to the macroscopic harmonic signal becomes marginal in a typical experiment (tightly focused Gaussian beam). Therefore, any HHG experiment aimed to resolve their signature must seek the conditions where the macroscopic emission retains the details of the single-radiator spectra with enough fidelity. Due to its non-perturbative origin, high-order harmonics are emitted with phases that depend on the phase as well as on the intensity of the driving field [36–38]. Hence, optimal phase matching will occur when the spatial variations of these two parameters are minimal. As it has been recently pointed out, phase matching is a two-dimensional problem, where not only phase variations along the longitudinal, but also along the transversal direction play a role [39, 40]. In this sense, Bessel beams (BB) constitute an optimal choice for phase matching, due to their constant phase profile along the two dimensions. They appear naturally in HHG experiments in hollow waveguides, and they are excellent to reach optimal longitudinal phase matching conditions [3, 41–43]). On the other hand, flat-top beams (FTB)

are special beams for which the intensity and phase remains almost constant in a limited spatial volume around the focus and, therefore, are specially attractive to reduce phase mismatch due to intensity gradients found in non-perturbative harmonic generation. FTB can be generated through spatial shaping of intense femtosecond beams and their potential to generate efficiently high-order harmonics has been reported recently [44, 45].

Figs. 2a and 2b show the transversal and longitudinal profiles (amplitude in solid lines and phase in dashed lines) of a BB (green), Gaussian beam (blue), and a FTB (red). The BB is represented by a plane wave modulated by the slowly varying transverse amplitude (written in cylindrical coordinates) [46]

$$A(\rho, z) = E_0 J_0 \left(2.405\rho/a\right) \exp\left(ikz\right) \quad (1)$$

where E_0 is the field amplitude, J_0 is the zero-order Bessel function, and a is the transversal width of the beam, equivalent to the radius of the waveguide in which the beam propagates. We implement the FTB as a superposition of Gaussian beams [47], propagating along the z axis as a plane wave modulated by the slowly varying transverse amplitude (written in cylindrical coordinates)

$$A_M(\rho, z) = E_0 \exp\left(ikz\right) \sum_{m=1}^{M} \alpha_m \frac{W_{0,m}}{W_m(z)} \exp\left[-\frac{\rho^2}{W_m^2(z)}\right] \times$$
$$\exp\left[ik\frac{\rho^2}{2R_m(z)} - i\zeta_m(z)\right], \quad (2)$$

where M is the total number of Gaussian beams considered, $W_m(z) = W_{0,m}[1 + (z/z_{0,m})^2]^{1/2}$ is the beam width, $W_{0,m}$ is the beam waist of the m-th component given by $W_{0,m} = W_{0,1}(m\beta)^{-1/2}$, with $W_{0,1} = (\lambda z_{0,1}/\pi)^{1/2}$. Correspondingly, the Rayleigh range of the m-th order is given by $z_{0,m} = \pi W_{0,m}^2 \lambda^{-1}$. The scaling factor β is given by $\beta = \sum_{m=1}^{M} \alpha_m/m$ where α_m is the binomial coefficient [47]. $R_m(z) = z[1 + (z_{0,m}/z)^2]$ is the wavefront radius of curvature and $\zeta_m(z) = \tan^{-1}(z/z_{0,m})$ is the Gouy phase. Note that if $M = 1$ we recover the standard Gaussian beam expression. The spatial profiles plotted in panels (a) and (b) in Fig. 2 show that phase variations of BB and FTB around the focus are less significant than those shown by Gaussian beams. Also the transversal intensity variations are less pronounced near the focus, becoming BB and FTB the natural choices to obtain high-order harmonics under optimal phase matching conditions.

C. Macroscopic HHG simulations.

We compute harmonic propagation using the electromagnetic field propagator [48]. We discretize the target (gas cell or gas jet) into a set of elementary radiating volumes, and propagate the emitted field $\mathbf{E}_j(\mathbf{r}_j, t)$ to the far-field detector,

$$\mathbf{E}_j(\mathbf{r}_d, t) = \frac{q_j \mathbf{s}_d}{c^2 |\mathbf{r}_d - \mathbf{r}_j|} \times \left[\mathbf{s}_d \times \mathbf{a}_j \left(t - \frac{|\mathbf{r}_d - \mathbf{r}_j|}{c}\right)\right] \quad (3)$$

where $\mathbf{s}_d$ is the unitary vector pointing to the detector, and $\mathbf{r}_d$ and $\mathbf{r}_j$ are the position vectors of the detector and of the elementary radiator j, respectively. Equation (3) assumes the harmonic radiation to propagate with the vacuum phase velocity, which is a reasonable assumption for high-order harmonics. Finally the total field at the detector is computed as the coherent addition of these elementary contributions. Propagation effects in the fundamental field, such as the production of free charges, the refractive index of the neutrals, the group velocity walk-off [49], as well as absorption in the propagation of the harmonics, are also taken into account.

For the case of intense fields the computation of the dynamics of the elementary radiators is not trivial, as the interaction is non-perturbative. Due to the large number of radiators, using the exact numerical integration of the TDSE becomes extremely expensive, specially for mid-IR driving fields. Therefore, the use of simplified models is almost mandatory. For the case of intense fields, S-matrix approaches combined with the Strong-Field Approximation (SFA) [50–52] are demonstrated to retain most of the features of the HHG [53, 54]. We have recently developed an extension of the standard SFA, hence we will refer it as SFA+. The total acceleration of the j radiator ($\mathbf{a}_j$) is found from two contributions, a_b and a_d, the first being the standard SFA expression, and the later being a correction due to the instantaneous dressing of the ground state. Or method computes the dipole acceleration directly from the superposition of the contributions of each Volkov wave, each can be integrated separately as an ordinary 1D equation, leading to a very efficient algorithm [55, 56].

Figure 2c shows the time-frequency analysis from the single-atom SFA+ calculation in helium for the same case as the TDSE results in Fig 1b. Both figures may be used as a benchmark for our SFA+ method. The photon energies and emission times, and therefore the harmonic phases, are well reproduced. On the other hand, the efficiency of the long trajectories relative to the short is underestimated in SFA+. Also, the yield of the cutoff harmonics compared to that of the plateau harmonics is higher in the TDSE calculations, and the the yield of the HOR compared to that of the first rescattering is substantially higher in the TDSE calculations. These differences should be attributted to the absence of Coulomb focussing of the electronic wavepacket in the SFA formulation, as discussed in [29]. Note that the color scaling of Figs. 1b and 2c is different, as the lower bound is set to the background noise level (that is lower in SFA+ calculations) .

In Figs. 2d to 2f, we show the results after propagation for the three beam profiles considered in this paper: (d) Gaussian beam with $W_{0,1} = 63.2$ μm, (e) BB with $a = 95$ μm and (f) FTB, using $M = 20$ and $W_{0,1} = 63.2$ μm. The 3D propagated harmonics are generated in a helium gas cell of thickness (L) of 0.1 mm (Gaussian beam), 2 mm (BB) and 1 mm (FTB), and at a pressure of 5 torr (gas density of 1.7×10^{17} atoms/cm^3). Note that the
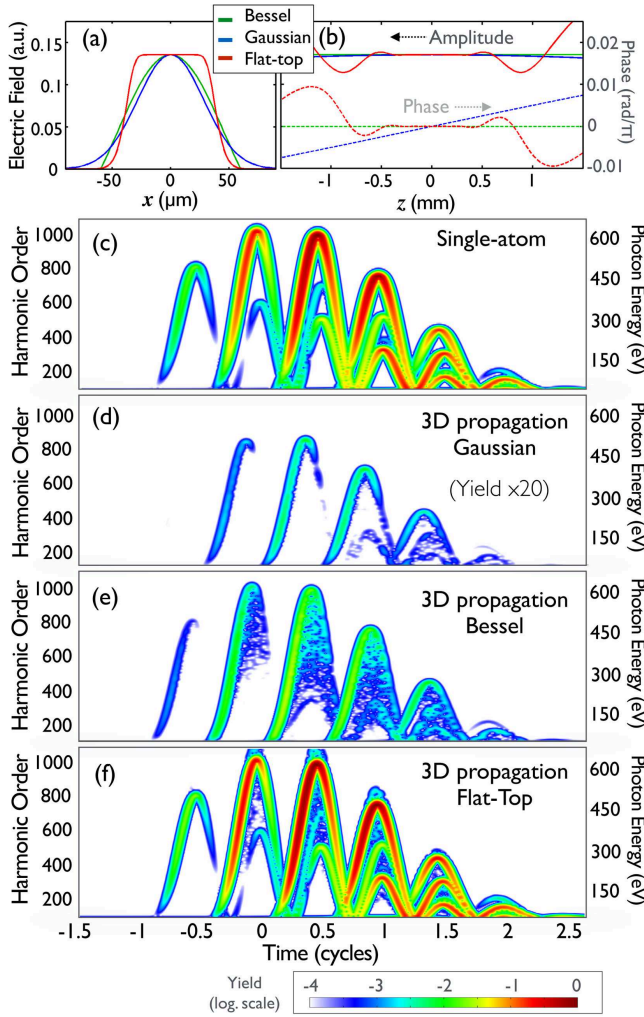
FIG. 2. (Color online) (a) Transversal and (b) longitudinal spatial field (solid lines) and phase (dashed lines) profiles at $\lambda = 2.0$ μm, for a BB with $a = 95$ μm (green), a Gaussian beam ($M = 1$, blue) and a FBM ($M = 20$, red), using a beam waist of $W_{0,1} = 63.2$ μm that gives a Rayleigh distance of $z_{0,1} = 6.28$ mm for the later two cases. (c) Time-frequency analysis of the HHG radiation from the single-atom SFA+ calculation for a laser pulse of 2.0 μm, using $\Delta\omega = 10\omega_0$. The rest of parameters of the laser pulse are as in Fig. 1. In panels (d) to (f) we show the results including macroscopic 3D propagation when using a Gaussian beam (d), a BB (e), and a FTB (f). The 3D propagated harmonics are generated in a helium gas cell of thickness (L) of 0.1 mm (Gaussian beam), 2 mm (BB) and 1 mm (FTB), at a pressure of 5 torr (gas density of 1.7×10^{17} atoms/cm^3). In the Gaussian beam case (d), the gas cell is placed 3 mm after the focus to achieve favorable phase-matching conditions, and the time-frequency yield is multiplied by a factor of 20 for better comparison with (e) and (f). In the case of the FTB (f) the gas cell is placed at the focus.

longitudinal phase variation of the Gaussian beam (Fig. 2b) limits the selection of the ratio between the target thickness and the Rayleigh range, $\alpha = L/z_{0,1}$. In our case, $z_{0,1} = 6.28$ mm, and then $\alpha = 1.6\%$. The use of larger α limits dramatically the efficiency of the high-order harmonics due to longitudinal phase-matching for the laser pulse parameters considered. In addition, in the Gaussian beam case, the gas cell is placed 3 mm after the focus, so favorable longitudinal phase-matching conditions are met due to the compensation of the Gouy and the intrinsic harmonic-phase gradients [36, 37]. On the other hand, in the case of the FTB, according to Fig. 2b, the gas cell thickness is chosen to be $L = 1$ mm and it is placed at the focus, where the longitudinal variations of the amplitude and phase are minimal (see Fig. 2b).

The results clearly show how phase matching modifies the macroscopic build-up of high-order harmonics. First, the use of Gaussian beams limits substantially the efficiency of the generated harmonics due to the transverse and longitudinal phase and amplitude variations of the driving field. As it has been showed previously, HOR are strongly suppressed due to phase-matching [28]. Note that the maximum photon energy obtained is lower than the other cases as the gas cell is placed 3 mm after the focus position.

Second, the use of BB (Fig. 2d) allows for the generation of brighter harmonics, although it introduces phase mismatch through the variations of the transversal intensity profile [39], since the beam phase is constant. In this case, short trajectory contributions (positive slope of the time-frequency structure) survive phase-matching, as it has been reported previously [3], and the signature of HOR is also diminished.

Finally, the use of focalized FTB (Fig. 2e) has a reduced spatial intensity variation (whereas keeping the phase variation small as compared to a Gaussian beam) and, consequently, phase mismatch is strongly weakened. In this case, the macroscopic yield retains the details of the single-source emission (Fig. 2c). Note that the quantitative comparison of the HHG yield between Figs. 2d to 2f depends on the particular choices of the transversal (a in the BB, and $W_{0,1}$ in the Gaussian beam and FTB), and longitudinal (target length) beam parameters. Our calculations show that the single-source features in the macroscopic target emission with FTB are preserved to the point to retain the spectral contributions of HOR.

III. TIME-FREQUENCY UNCERTAINTY: MID-IR PREFERENCE FOR HIGH-ORDER RESCATTERING DETECTION

A second important aspect when resolving HOR is the choice of the driving-wavelength. It has already been pointed out that, at the single-radiator level, HOR seem to emerge more distinctly using mid-IR driving fields [11, 29, 30]. To explore this point we have compared the results from the TDSE calculation at 2 μm wavelength,
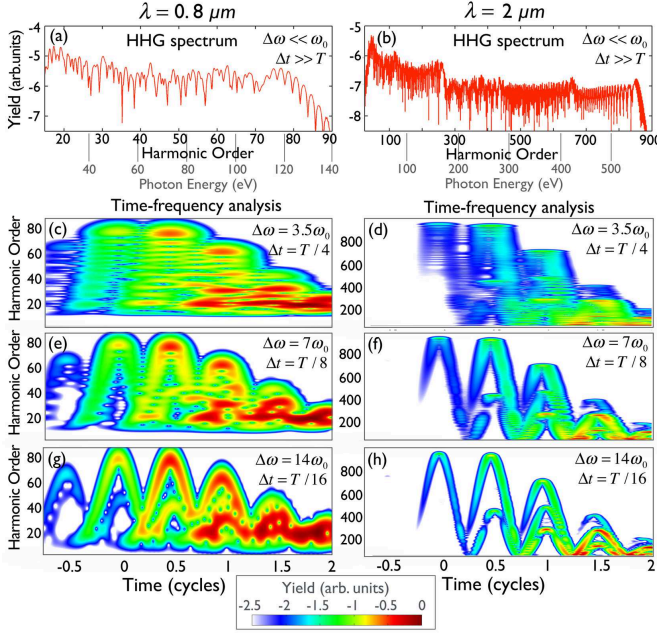
FIG. 3. (Color online) HHG spectra (first row), and time-frequency analysis (second to fourth rows) driven in helium at 0.8 μm (first column), and 2 μm (second column). The laser pulse is modeled by a $\cos^2$ envelope, 6 cycles full width and peak intensity of 5×10^{14} W/cm^2. From row to row, the spectral ($\Delta\omega$) and corresponding temporal (Δt) FWHM of the Gaussian windows in the TFA are $(3.5\omega_0, T/4)$, $(7\omega_0, T/8)$, and $(14\omega_0, T/16)$ being ω_0 the fundamental frequency and T the laser period. Note that both the spectra and TFA are in logarithmic scale.

already shown in Fig. 1b, with the same case at 0.8 μm. We show the respective harmonic spectra in Figs. 3a and 3b. The rescattering energies scale linearly with the electron's ponderomotive energy $U_P \propto I\lambda^2$. Therefore, the harmonic spectra extends deeper into XUV wavelengths with increasing the driving field's wavelength. Panels 3(c) to 3(e) and 3(f) to 3(h) show the time-frequency analysis of the harmonic signals for the two wavelengths considered, for different widths of the spectral amplitude window ($\Delta\omega$). It is quite evident that HOR can not be properly resolved for the 0.8 μm driving field with any choice of spectral window, while they are clearly resolved for the 2 μm driving field if sufficiently wide spectral windows are used. This is a natural consequence of the time-frequency indetermination.

Let us now explore this phenomena in quantitative terms. Assuming a Gaussian window profile, the minimum time resolution (separation of the Gaussian distributions needed to have a $1/e$ contrast) is of 1.56Δ, Δ being the FWHM of the Gaussian (Δt for the temporal window and $\Delta\omega$ for the spectral one). Note in Fig. 1 that a given harmonic is typically emitted during a half-cycle of the driving field by a pair of trajectories for each rescattering order. Therefore, if up to n rescattering or-

ders are to be resolved in time, the visibility criterium for rescatterings during one-fourth of a cycle leads to $n \times 1.56\Delta t \lesssim T/4$, and therefore $\Delta t \lesssim T/6.24n$. As presented in section II, the uncertainty relation for the FWHM of the Gaussian windows reads $\Delta t\Delta\omega = 5.5$, and therefore $\Delta\omega \gtrsim 34.32n/T$.

On the other hand, the application of the same visibility criterium in the spectral domain, requires an energy resolution in the harmonic spectrum of $\Delta E \gtrsim 1.56\hbar\Delta\omega = 53.54n/T$. If the maximum rescattering energy over one half-cycle of the driving field is E_{max}, the observation of n rescattering orders in the harmonic spectrum requires $\Delta E \leq E_{max}/n$. Expressing E_{max} in U_P units, the wavelength in μm, and the intensity in W/cm^2, the driving wavelength required to resolve n rescattering orders is,

$$\lambda_{\mu m} > 4.9 \times 10^4 n^{2/3} \left(E_{max}I\right)^{-1/3} \qquad (4)$$

For instance, for the case of Fig. 3, in order to resolve the three rescattering orders that take place at the time-interval from 0.7T to 1.2T a driving laser with wavelength of $\lambda \gtrsim 1$ μm is needed (in this case, $E_{max} = 2.19U_P$ which corresponds to $\sim$ 700th harmonic order, $I = 5 \times 10^{14}$ $W\,cm^{-2}$, and $n = 3$). This lower limit illustrates that long mid-IR wavelength driving lasers are required in order to resolve HOR.

Finally, even though the proper choice of beam profile and wavelength provides the physical conditions for the observation of HOR radiation, unraveling their signature in the harmonic spectrum (Figs. 3a and 3b), is far from trivial. HOR harmonics present energies in the mid-part of the spectrum (*plateau*) and, thus, their observation is hindered by the contributions of the lowest order rescatterings over the whole interaction history. On the other hand, the identification of HOR in the temporal domain turns out to be also very difficult, as depicted in Fig. 4a, where we show the attosecond pulse train obtained from the Fourier transform of the single-atom harmonic spectrum presented in Fig. 3b. Nevertheless, it is possible to obtain a distinct spectral signature by selecting only those temporal events occurring over half a cycle of the driving field. In such case, the energy distribution of the HOR is ordered enough to leave a clear imprint in the harmonic signal.

Figs. 4b and 4c show the propagated spectra of the individual harmonic bursts (on a linear scale) for the BB (green) and FTB (red) considered before at 2 μm. These results correspond to the spectra of the bursts generated within (b) $0.7 < t_0/T < 1.2$ and (c) $1.2 < t_0/T < 1.7$ in Figs. 2d and 2e, for the BB (green) and FTB (red) respectively. We can identify different peaks corresponding to the first, second and third rescattering energies, that can only be macroscopically resolved when using the FTB. As commented above, note that if TDSE is used when computing HHG, the yield of the higher-order rescatterings would be higher.

It has been shown in recent experiments that the harmonic bursts can be angularly isolated from the attosecond train in the far-field, an effect termed attosecond
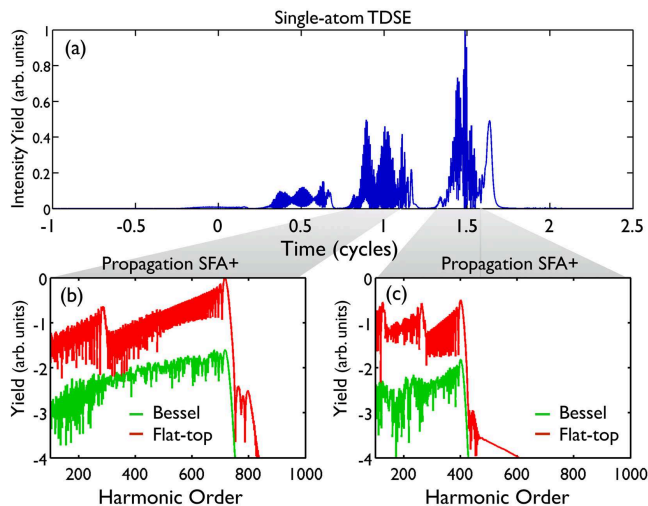
FIG. 4. (Color online) (a) Single-atom HHG attosecond pulse train obtained from the Fourier transform of the single-atom harmonic spectrum presented in Fig. 3b. Panels (b) and (c) show the propagated spectra (in logarithmic scale) of two individual harmonic bursts (b, $0.75 < t_0/T < 1.25$ and c, $1.25 < t_0/T < 1.75$) for the Bessel (green), and flat-top (green) beams considered before at 2 μm. The rest of parameters are the same as in Figs. 2e and 2f.

lighthouse [57, 58]. The discrimination power is known to increase with the wavelength and to be optimal for short pulses, therefore, it is an optimal technique for measuring the spectra of the separated bursts, and therefore, for identifying HOR signatures. In addition, another technique has recently been proposed to identify HOR by using a VUV pump to temporally control the emergence of HHG radiation, and thus the relevance of HOR [59].

In conclusion, we have shown that mid-IR flat-top laser beams are ideal candidates to identify the signatures of high-order rescatterings in HHG, in order to overcome the limitations imposed by phase-matching and by the time-frequency uncertainty. We provide a route to experimentally identify HOR, opening the prospective for their possible applications. In this sense, we should stress that recent developments of flat-top beams in fibers [60, 61], combine the optimal longitudinal phase-matching properties of Bessel beams with the transversal ones of flat-top beams, a promising perspective to obtain high-flux multiple-rescattering emission.

[1] A. McPherson, G. Gibson, H. Jara, U. Johann, T. S. Luk, I. A. McIntyre, K. Boyer, and C. K. Rhodes, et al. J Opt Soc Am B **4** 595-601 (1987).
[2] X.F. Li, A. L'Huillier, M. Ferray, L. A. Lompré, G. Mainfray, Phys. Rev. A **39** 5751?5761 (1989).
[3] T. Popmintchev, M. Chen, D. Popmintchev, P. Arpin, S. Brown, S. Ališauskas, G. Andriukaitis, T. Balčiunas, O. Mücke, A. Pugzlys, A. Baltuška, B. Shim, S. E. Schrauth, A. Gaeta, C. Hernández-García, L. Plaja, A. Becker, A. Jaroń-Becker, M. M. Murnane, and H. C. Kapteyn, Science **336**, 1287 (2012).
[4] K. J. Schafer, B. Yang, L. F. DiMauro, and K. C. Kulander, Phys. Rev. Lett. **70**, 1599 (1993).
[5] P. B. Corkum, Phys. Rev. Lett. **71**, 1994 (1993).
[6] I. P. Christov, M. M. Murnane and H. C. Kapteyn, Phys. Rev. Lett. **78**, 1251 (1997).
[7] P. M. Paul, E. S. Toma, P. Breger, G. Mullot, F. Augé, Ph. Balcou, H. G. Muller, and P. Agostini, Science **292**, 1689 (2001).
[8] R. Kienberger, E. Goulielmakis, M. Uiberacker, A. Baltuška, V. Yakovlev, F. Bammer, A. Scrinzi, Th. Westerwalbesloh, U. Kleineberg, U. Heinzmann, M. Drescher and F. Krausz, Nature **427**, 817 (2004).
[9] M. Lewenstein, P. Salières, and A. LHuillier, Phys. Rev. A **52**, 4747 (1995).
[10] A. Zaïr, M. Holler, A. Guandalini, F. Schapper, J. Biegert, L. Gallmann, U. Keller, A. S. Wyatt, A. Monmayrant, I. A. Walmsley, E. Cormier, T. Auguste, J. P. Caumes, and P. Salières, Phys. Rev. Lett. **100**, 143902 (2008).
[11] C. Hernández-García, J.A. Pérez-Hernández, T. Popmintchev, M.M. Murnane, H.C. Kapteyn, A. Jaroń-Becker, A. Becker, and L. Plaja, Phys. Rev. Lett. **111**, 033002 (2013).
[12] G. Andriukaitis, T. Balčiunas, S. Ališauskas, A. Pugzlys, A. Baltuška, T. Popmintchev, M.-C. Chen, M. M. Murnane, and H. C. Kapteyn, Opt. Lett. **36**, 2755–2757 (2011).
[13] P. Malevich, G. Andriukaitis, T. Flöry, A. J. Verhoef, A. Fernández, S. Ališauskas, A. Pugzlys, A.Baltuška, L. H. Tan, C. F. Chua, and P. B. Phua, Opt. Lett. **38**, 2746–2749 (2013).
[14] I. Pupeza, D. Sánchez, J. Zhang, N. Lilienfein, M. Seidel, N. Karpowicz, T. Paasch-Colberg, I. Znakovskaya, M. Pescher, W. Schweinberger, V. Pervak, E. Fill, O. Pronin, Z. Wei, F. Krausz, A. Apolonski, and J. Biegert, Nature Phot. **9** 721–724 (2015).
[15] E.J. Takahashi, T. Kanai, K. L. Ishikawa,Y. Nabekawa, and K. Midorikawa, Phys. Rev. Lett. **101**, 253901 (2008).
[16] M.C. Chen, P. Arpin, T. Popmintchev, M. Gerrity, B. Zhang, M. Seaberg, D. Popmintchev, M.M. Murnane and H.C. Kapteyn, Phys. Rev. Lett. **105**, 173901 (2010).
[17] M.-C. Chen, C. Mancuso, C. Hernández-García, F. Dollar, B. Galloway, D. Popmintchev, P.-C. Huang, B. Walker, L. Plaja, A. A. Jaron-Becker, A. Becker, M. M. Murnane, H. C. Kapteyn, and T. Popmintchev, Proc.

Natl. Acad. Sci. USA **111**, E2361-E2367 (2014).

[18] S. L. Cousin, F. Silva, S. Teichmann, M. Hemmer, B. Buades, and J. Biegert, Opt. Lett. **39**, 5383–5386 (2014).

[19] S. Baker, J. S. Robinson, C. A. Haworth, H. Teng, R. A. Smith, C. C. Chirila, M. Lein, J. W. G. Tisch, and J. P. Marangos, Science **21** 312 (2006).

[20] C. I. Blaga, F. Catoire, P. Colosimo, G. G. Paulus, H. G. Muller, P. Agostini, and L. F. DiMauro, Nat. Phys. **5**, 335 (2009).

[21] C. Liu, K. Z. Hatsagortsyan, Phys. Rev. Lett. **105**, 113003 (2010).

[22] T.-M. Yan, S. V. Popruzhenko, M. J. J. Vrakking, and D. Bauer, Phys. Rev. Lett. **105**, 253002 (2010).

[23] A. Kästner, U. Saalmann, and J. M. Rost, Phys. Rev. Lett. **108**, 033201 (2012).

[24] D. D. Hickstein, P. Ranitovic, S. Witte, X. M. Tong, Y. Huismans, P. Arpin, X. Zhou, K. E. Keister, C. W. Hogle, B. Zhang, C. Ding, P. Johnsson, N. Toshima, M. J. J. Vrakking, M. M. Murnane, and H. C. Kapteyn, Phys. Rev. Lett. **109**, 073004 (2012).

[25] P. Moreno, L. Plaja, V. Malyshev, and L. Roso, Phys. Rev. A **51**, 4746 (1995).

[26] T. Brabec, M. Y. Ivanov, and P. B. Corkum, Phys. Rev. A **54**, R2551 (1996).

[27] G. L. Yudin and M. Y. Ivanov, Phys. Rev. A **63**, 033404 (2001).

[28] A.-T. Le, H. Wei, C. Jin, V. N. Tuoc, T. Morishita, and C. D. Lin, Phys. Rev. Lett. **113**, 033001 (2014).

[29] J. Tate, T. Auguste, H. G. Muller, P. Salières, P. Agostini, and L. F. Di Mauro, Phys. Rev. Lett. **98**, 013901 (2007).

[30] L. He, Y. Li, Z. Wang, Q. Zhang, P. Lan, and P. Lu, Phys. Rev. A **89**, 053417 (2014).

[31] P. Antoine, B. Piraux,and A. Maquet, Phys. Rev. A **51**, R1750 (1995).

[32] X. M. Tong and S. I. Chu, Phys. Rev. A **55**, 3406 (1997)

[33] X. M. Tong and C. D. Lin, J. Phys. B: At. Mol. Opt. Phys. **38**, 2593 (2005).

[34] M. B. Gaarde, J. L. Tate, and K. J. Schafer, J. Phys. B: At. Mol. Opt. Phys. **41**, 132001 (2008).

[35] T. Popmintchev, M.C. Chen, P. Arpin, M. M. Murnane and H. C. Kapteyn, Nature Photon. **4**, 822 (2010).

[36] P. Salières, A. L'Huillier, and M. Lewenstein, Phys. Rev. Lett. **74**, 3776 (1995).

[37] P. Balcou, P. Salières, A. L'Huillier, and M. Lewenstein, Phys. Rev. A **55**, 3204 (1997).

[38] C. Hernández-García and L. Plaja, J. Phys. B: At. Mol. Opt. Phys. **45**, 074021 (2012).

[39] C. Hernández-García, I. J. Sola, and L. Plaja, Phys. Rev. A **88**, 043848 (2013).

[40] C. Hernández-García, W. Holgado, L. Plaja, B. Alonso, F. Silva, M. Miranda, H. Crespo, and I. J. Sola, Opt. Exp.**23**, 21497–21508 (2015).

[41] T. Popmintchev, M.C. Chen, A. Bahabad, M. Gerrity, P. Sidorenko, O. Cohen, I. P. Christov, M. M. Murnane, and H. C. Kapteyn, Proc. Natl. Acad. Sci. USA **106**, 10516 (2009).

[42] A. Rundquist, C.G. Durfee III, Z. Chang, C. Herne, S. Backus,M. M. Murnane, and H. C. Kapteyn, Science **280**, 1412-1415 (1998).

[43] C.G. Durfee, A.R. Rundquist, S. Backus, C. Herne, M. M. Murnane, and H. C. Kapteyn, Phys. Rev. Lett. **83**, 2187 (1999).

[44] W. Boutu, T. Auguste, O. Boyko, I. Sola, Ph. Balcou, L. Binazon, O. Gobert, H. Merdji, C. Valentin, E. Constant, E. Mével, and B. Carré, Phys. Rev. A **84**, 063406 (2011).

[45] A. Dubrouil, Y. Mairesse, B. Fabre, D. Descamps, S. Petit, E. Mével, and E. Constant, Opt. Lett. **36**, 2486 (2011).

[46] E. A. J. Marcatili and R. A. Schmeltzer, Bell Syst. Tech. J. **43**, 1783 (1964).

[47] Y. Li, Opt. Commun. **206**, 225-234 (2002).

[48] C. Hernández-García, J. A. Pérez-Hernández, J. Ramos, E. Conejero Jarque, L. Roso, and L. Plaja, Phys. Rev. A **82**, 033432 (2010).

[49] C. Hernández-García, T. Popmintchev, M.M. Murnane, H.C. Kapteyn, L. Plaja, A. Becker, and A. Jaroń-Becker, submitted (2015).

[50] L. V. Keldysh, Zh. Eksp. Teor. Fiz. **47**, 1945 (1964) [Sov. Phys. JETP **20**, 1307 (1965)].

[51] F. H. M. Faisal, J. Phys. B **6**, L89 (1973).

[52] H. R. Reiss, Phys. Rev. A **22**, 1786 (1980).

[53] W. Becker, A. Lohr, M. Kleber and M. Lewenstein, Phys. Rev. A **56**, 645 (1997).

[54] M. Lewenstein, Ph. Balcou, M. Yu. Ivanov, A. L'Huillier, P. B. Corkum, Phys. Rev. A **49**, 2117 (1994).

[55] J. A. Pérez-Hernández, L. Roso, and L. Plaja, Opt. Express **17**, 9891 (2009).

[56] J. A. Pérez-Hernández, C. Hernández-García, J. Ramos, E. Conejero, L. Plaja and L. Roso, "New Methods For Computing High-Order Harmonic Generation and Propagation," Book Chapter: Progress in Ultrafast Intense Laser Science VII, (pp 145-162), Springer (2011).

[57] H. Vincenti and F. Quéré, Phys. Rev. Lett. **108**, 113904 (2012).

[58] J. A. Wheeler, A. Borot, S. Monchocé, H. Vincenti, A. Ricci, A. Malvache, R. Lopez-Martens, and F. Quéré, Nature Phot. **6**, 829-833 (2012).

[59] M. R. Miller, C. Hernández-García, A. Jaroń-Becker, and A. Becker, Phys. Rev. A **90**, 053409 (2014).

[60] C. Valentin, P. Calvet, Y. Quiquempois, G. Bouwmans, L. Bigot, Q. Coulombier, M. Douay, K. Delplace, A. Mussot, and E. Hugonnot, Opt. Exp. **21**, 23250 (2013).

[61] F. Kong, G. Gu, T. W. Hawkins, J. Parsons, M. Jones, C. Dunn, M. T. Kalichevsky-Dong, K. Wei, B. Samson, and L. Dong, Opt. Exp. **21**, 32371-32376 (2013).